TÜBİTAK

Turkish Journal of Earth Sciences

http://journals.tubitak.gov.tr/earth/

Research Article

Turkish J Earth Sci
(2020) 29: 538-549

doi:10.3906/yer-1912-7

Coseismic surface deformation and fault model of the 27 May 2017 Mw 5.2 Saruhanlı-Manisa (western Turkey) earthquake from InSAR

Ahmet M. AKOĞLU*
Department of Geological Engineering, Faculty of Mines, İstanbul Technical University, İstanbul, Turkey

Received: 10.12.2019 • **Accepted/Published Online:** 08.01.2020 • **Final Version:** 16.03.2020

Abstract: The shortened revisit times and accurate orbits of the new generation of radar satellites like Sentinel-1 improved the applicability of the synthetic aperture radar interferometry (InSAR) technique to investigate more moderate size events. Here the technique is used to characterize the 27 May 2017 Mw 5.2 Saruhanlı (Manisa) earthquake that took place in western Turkey in the Gediz Graben. Though seismological focal mechanism solutions of the earthquake clearly indicated that the event is due to normal faulting, the nodal plane ambiguity and the presence of two closely located faults in the epicentral region prevented the assessment of the causative fault. Data from the Sentinel-1 radar satellites and subsequent modeling indicate that a 9-km-long, NE-dipping fault had ruptured during the earthquake with the shallow rupture coinciding with the Ozanca Fault in the region.

Key words: Synthetic aperture radar interferometry (InSAR), coseismic model, normal faulting, western Turkey, Manisa

1. Introduction

Dominated by the interaction between the Arabian, Eurasian, and Nubian plates, Anatolia is one of the most seismically active continental regions of the world. While the North and East Anatolian fault zones that act as major boundaries between these plates are now very well known and studied, the comparatively short and mostly blind networks of normal faults that produce frequent moderate events especially in western Anatolia and the seismic hazards associated with them are still poorly understood. As evident from Figure 1, which shows the M > 5 events in the Aegean region for the year 2017, several moderately sized events occur every year on normal faults in the region, which could provide new insights if studied in detail.

The synthetic aperture radar interferometry (InSAR) technique is being used extensively for studying coseismic events in Anatolia since the 1995 Mw 6.4 Dinar earthquake (Wright et al., 1999). In the last two decades, in addition to studies focusing on the major earthquakes of 1999 in İzmit-Düzce (Çakir et al., 2003; Konca et al., 2010) and 2011 in Van (Akoğlu et al., 2018 and references therein) and creep events along the North and East Anatolian faults (Cakir et al., 2005; Cavalié and Jónsson, 2014), InSAR has helped geoscientists study and document several previously unknown active faults of Anatolia and their corresponding parameters (Cakir and Akoglu, 2008; Dogan et al., 2014). However, the technique could not be applied to study M < 6 events, with the exception of the 2007 Mw 5.7 Sivrice-Elazığ earthquake (Şentürk et al., 2019), due to factors such as the long revisit times of the available radar satellites, decorrelation, and large baselines.

With the launch of the Sentinel constellation's second radar satellite in 2016, now a revisit time of 6 days is possible for most of the active tectonic regions of the world, the Anatolian plate being one of them. Shortened revisit times and accurate orbits that are now possible with this new generation of satellites not only makes it possible to respond to earthquakes much faster than before, but also increases the chance of studying these moderately sized events onshore in detail due to the overall increase in interferometric coherence (Funning and Garcia, 2019).

In this manuscript an InSAR-based analysis of one of these moderately sized events shown in Figure 1, the 27 May 2017, Mw 5.2 Saruhanlı earthquake is presented making use of this rich Sentinel-1 archive. The main question regarding this event is the nodal plane ambiguity that arises from the fact that the epicentral region is surrounded by two adjacent parallel normal faults with only 5 km of distance between them. Yet another question arises due to the occurrence of four subsequent events within the first 24 h with magnitudes between 4.5 and 5.0 in the very same region (Table 1). The manuscript starts with a brief introduction of the seismotectonics

* Correspondence: akoglua@outlook.com

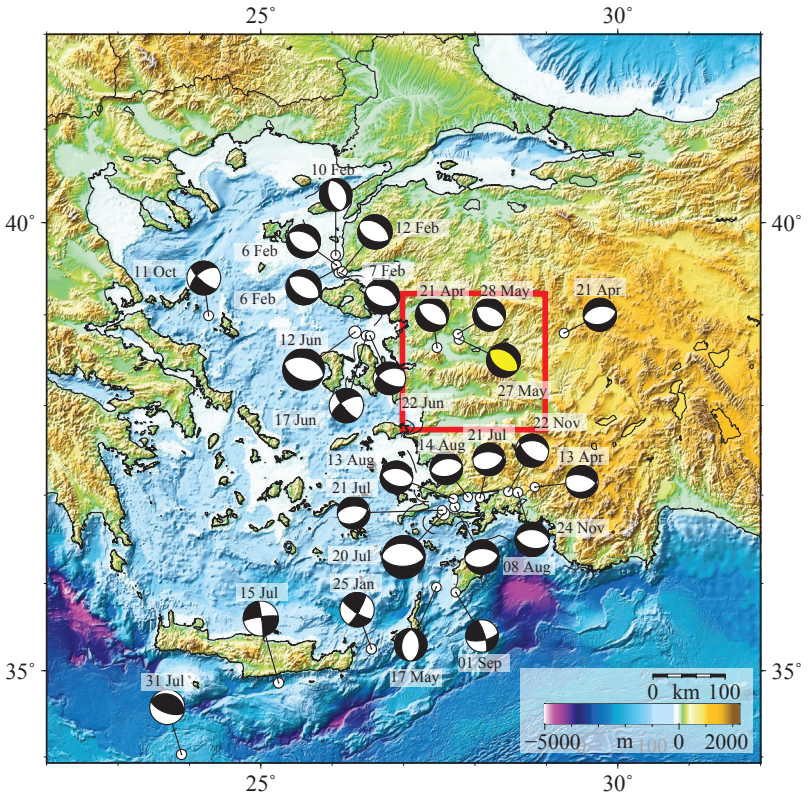

Figure 1. The focal mechanism solutions of the M > 5 earthquakes in western Turkey and the Aegean for the year 2017 providing an indication of the intensity and overall nature of the seismic activity in the region, emphasizing the importance of studying moderate events with InSAR. The solutions are from the Global CMT project's catalogue (Ekström et al., 2012). The bathymetry is from the GEBCO 2019 grid (GEBCO Compilation Group, 2019). The focal mechanism solution of the 27 May 2017 Saruhanlı earthquake is shown in yellow. The red rectangle represents the area shown in Figure 2.

of the epicentral region, followed by a description of the InSAR dataset used to address these questions. The text is concluded with a discussion of the resulting model, the causative fault, the calculated Coulomb stress changes, and the importance of InSAR for studying these moderate events for assessing the seismic hazard in the region.

2. Tectonic setting and the 27 May 2017 earthquake

The active tectonics of Anatolia and the adjacent regions are mainly controlled by the convergence of the Eurasian, Nubian, and Arabian plates (Reilinger et al., 2010; Jolivet et al., 2013). The postcollisional convergence of Anatolia and Arabia in the east and the Hellenic Subduction in the west forms the main boundary conditions of this actively deforming region (McKenzie, 1972). There are multiple suggestions explaining the deformation of the Western Anatolia Extensional Province (or the Anatolian-Aegean Region), including (a) the obstruction of the westward motion of Anatolia due to the southwesterly bend in the course of the North Anatolian Fault (Dewey and Şengör, 1979; Şengör et al., 1985); (b) back-arc spreading caused by the S-SW rollback of the Hellenic Trench (Le Pichon and Angelier, 1979, 1981; Royden, 1993; Reilinger et al., 2006, 2010; Le Pichon and Kreemer, 2010); (c) orogenic collapse, in which the extension started by the spreading and thinning of over-thickened crust (Seyitoğlu and Scott, 1991; Seyitoğlu et al., 1992); and (d) combinations of these mechanisms (Koçyiğit et al., 1999; Philippon et al., 2014). The mean elevation has decreased from ~3 km to 500 m and has become submarine under the Aegean Sea, suggesting about 3 cm/year of lithospheric stretching since 11 Ma (Şengör and Zabcı, 2019). The total amount of extension was estimated to be on the order of 50% in the Aegean (McKenzie, 1978) and at least about 30% in western Turkey (Şengör, 1978). This extension has generated 6 major east-west oriented rifts (Şengör and Zabcı, 2019). Detailed fault maps show that these major rifts form complex structural features, especially in their hanging walls, composed of cross faults (i.e. transfer faults, irrotational and rotational accommodation faults) that are oriented at high angles to the strike of the major normal faults (Şengör, 1987). In the Manisa region (Figure 2), where the May 2017 earthquake

Table 1. Source parameters of the mainshock and the two events that occurred on the following day (Figure 3). AFAD, Disaster and Emergency Management Authority of Turkey; GCMT, Global Centroid Moment Tensor Project (Ekström et al., 2012); GFZ: German Research Centre for Geosciences, Potsdam; INGV: Istituto Nazionale di Geofisica e Vulcanologia Regional Centroid-Moment Tensors Catalog (Pondrelli, 2002) USGS, U.S. Geological Survey. The discrepancy between the geodetic and seismic moments for the mainshock are discussed in the text.

Event	Source	Strike (°)	Dip (°)	Rake (°)	Depth (km)	Mo (10^{16} Nm)	Mw
27/05/17 15:53 Mainshock	AFAD	135 298	36 55	–76 –100	5.1	4.87	5.1
	GFZ	135 309	44 46	–85 –93	10	-	5.1
	GCMT	125 304	46 44	–89 –91	12	7.23	5.2
	INGV	123 319	43 49	–102 –79	10	-	5.2
	USGS	123 301	32 58	–88 –91	5	4.79	5.1
	This study	121	52	Free (average: –87)	-	18.1	5.47
28/05/17 02:50 Aftershock #1	AFAD	112 311	35 56	–106 –79	5.2	0.622	4.5
	GFZ	129 315	47 43	–92 –85	10	-	4.6
28/05/17 02:52 Aftershock #2	AFAD	122 311	29 61	–98 –86	5.1	3.37	4.9
	GCMT	291 131	36 56	–107 –78	12.3	2.36	4.8
	GFZ	134 304	36 54	–81 –5	10	-	4.7
	USGS	108 321	31 63	–119 –74	3	2.159	4.82
28/05/17 04:38 Aftershock #3	AFAD	130 287	34 58	–71 –103	7.1	0.602	4.5
28/05/17 11:04 Aftershock #4	AFAD	124 306	27 63	–92 –89	5.2	5.068	5.0
	GCMT	132 290	41 51	–73 –104	12	3.9	5.0
	GFZ	134 303	41 49	–81 –96	10	-	4.9
	INGV	121 310	49 41	–96 –83	10	-	4.9
	USGS	117 319	38 54	–107 –77	4	2.489	4.86
21/04/17 14:12 Manisa-Şehzadeler earthquake	AFAD	274 157	52 60	–141 –45	13.2	1.315	4.7
	GCMT	300 125	36 54	–95 –87	12	5.69	5.1
	GFZ	306 127	39 51	–90 –88	10	-	5.0

took place, it is suggested that some of these high (or low) angle faults to the major rifts have formed within the stress regime of a larger tectonic belt, the sinistral İzmir-Balıkesir Transfer Zone (Özkaymak et al., 2013).

The 27 May 2017 earthquake took place at 18:53 (GMT+3) near the Saruhanlı town of Manisa, in an area that is surrounded by the Ozanca Fault to the west and Gölmarmara Fault to the east (Figure 3). The aftershocks were also confined to the same area. These two normal faults, which were both added to the General Directorate of Mineral Research and Exploration of Turkey's (MTA) active fault database in the last decade (Emre et al., 2013), trend in a NNW-SSE direction. The Gölmarmara Fault to the east is bounding the Gölmarmara basin that is part of a larger rift system, the Gediz Graben, which with the Küçük Menderes and Büyük Menderes grabens accommodates about 11 mm/year of extension in western Anatolia (Aktug et al., 2009). The Gediz Graben extends between Sarıgöl in the east and Salihli to the west (Figure 2), whereas west of Salihli, the whole system bifurcates into three subbasins, Kemalpaşa, Manisa, and Gölmarmara, respectively, from south to north (Özkaymak et al., 2013). The Gölmarmara Basin was previously studied using multispectral remote sensing, suggesting dominant NW-oriented lineaments within the region (Kavak, 2005; Kavak and Cetin, 2007). Recent geological field studies along the Ozanca Fault suggest that the NE-dipping high-angle fault is composed of three segments and has an oblique normal character (Eski, 2014; Altikulac, 2015).

3. InSAR dataset

The SAR satellites Sentinel 1A and 1B of the European Union's Copernicus Earth observation program, which were launched in 2014 and 2016, respectively, provide an extensive archive for Anatolia. Their improved revisit period of 6 days is essential for studying earthquakes in regions like western Anatolia, where signal coherence decreases dramatically with time due to agricultural activities.

After processing a series of interferograms using all the available Sentinel-1 data taken in the period 3 months before and after the earthquake, the pairs listed in Table 2

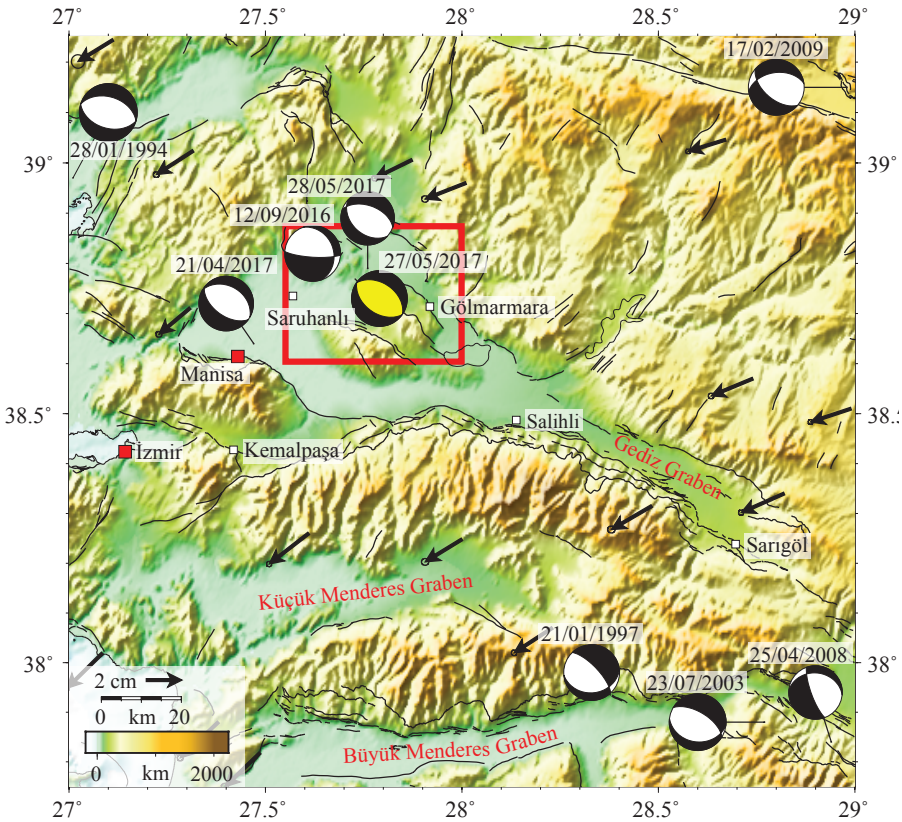

Figure 2. First close-up of the study area showing general tectonics of the study area with the focal mechanism solutions of the M > 5 earthquakes since 1994. The solutions are from the Global CMT project's catalogue (Ekström et al., 2012). The focal mechanism solution of the 27 May 2017 Saruhanlı earthquake is shown in yellow. The red rectangle represents the area shown in Figures 3 and 4. The black lines represent the faults from the active fault database of the General Directorate of Mineral Research and Exploration of Turkey (MTA) that was updated in 2013 (Emre et al., 2018). The black vectors are showing GPS velocities with respect to Eurasia (Aktug et al., 2009).

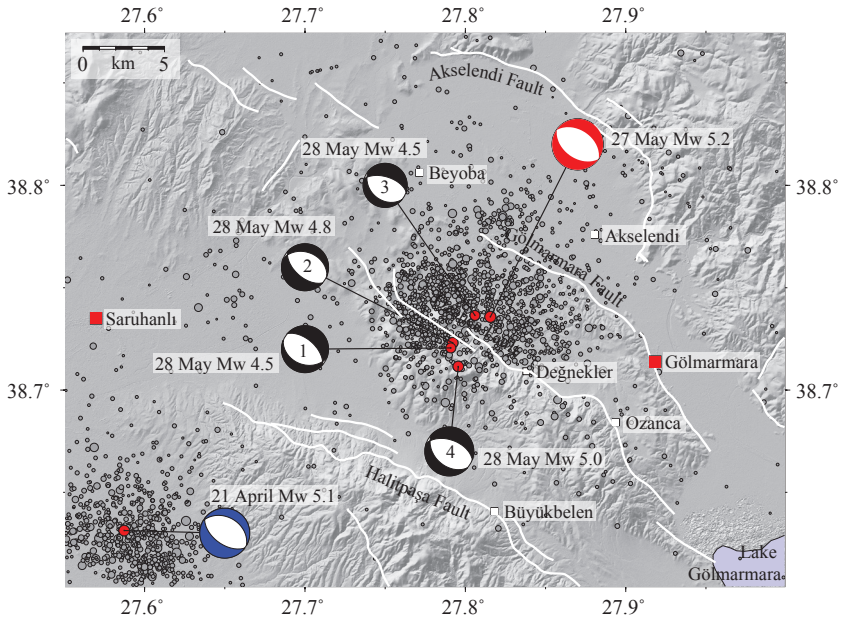

Figure 3. Second close-up of the study area with white lines representing the known active faults from Emre et al. (2018). The focal mechanism solutions are from the Global CMT project (Table 1) with the exception of aftershocks #1 and #3, where the solutions came from the Disaster and Emergency Management Authority of Turkey (AFAD) catalogue. Red solution denotes the mainshock. The gray circles represent the seismic activity from the same AFAD catalogue for 2017. The focal mechanism in blue and the related aftershocks in the bottom left corner of the image belong to the 21 April 2017 Mw 5.1 Şehzadeler-Manisa earthquake, which was not detected with InSAR owing probably to its reported depth, which is >10 km (Table 1, bottom row).

Table 2. SAR datasets used in this study. dT, Temporal baseline.

Dates (dd/mm/yyyy)	Orbit direction	Track	dT (days)	Wavelength (cm)
19/05/2017 – 31/05/2017	Descending	36	12	C (5.6)
25/05/2017 – 31/05/2017	Ascending	131	6	C (5.6)

that exhibit the minimum atmospheric contribution and the highest coherence were selected. The InSAR Scientific Computing Environment (ISCE) software (Rosen et al., 2015) is used to process the Sentinel-1 TOPS data with ESA's precise orbits as well as a TanDEM-X digital elevation model for topographical correction that provides a spatial resolution of 12 m. The calculated interferograms are presented in wrapped form in Figure 4. The unwrapped interferograms are subsampled using the quad-tree algorithm (Jónsson et al., 2002).

The overall pattern of deformation is quite similar for the descending and ascending interferograms where a semicircular set of fringes to the east of the Ozanca Fault are visible as expected from a dip-slip earthquake. Whereas three clear fringes on the hanging-wall can be counted on the descending interferogram, four fringes can be counted on the ascending one, leading to a peak-to-peak line of sight (LOS) displacement of ~11 cm on the surface.

As documented by several studies, a significant remaining drawback of the InSAR technique for active tectonics studies is the occurrence of atmospheric delays. Spatial and temporal variation of pressure, temperature, and humidity between radar scenes can cause phase delays in the interferograms. Despite the effort to select pairs with the lowest atmospheric contribution, there are still visible tropospheric signals worth mentioning in the interferograms that can affect modeling. Two of the popular approaches to deal with tropospheric delays are empirical model corrections to remove topography correlated tropospheric delays and corrections based on global numerical weather models (Merryman Boncori, 2019; Murray et al., 2019). As seen in Figure 4a, the descending interferogram, which was formed by radar scenes captured in the early morning, is less noisy with a signal mimicking the relief to the west of the Ozanca Fault. However, the elevation of the hill to the south (called

Karadağ Hill or North Çaldağ High) is only ~300 m and a correlation between phase and topography could not be found. The ascending interferogram formed by radar scenes captured early in the evening is superimposed with a stronger atmospheric signal that too is not correlated with the topography. Since the epicentral area is quite small, numerical weather models were not helpful for correcting these delays.

4. Coseismic model

For modeling, the analytical solutions of Okada (1985) are used to relate the InSAR measurements with dislocations along rectangular planes buried in a homogeneous and elastic half-space with constant material properties (Poisson's ratio of 0.25 and a rigidity modulus of 30 GPa). The modeling is performed in two stages and the methodology is similar to that of Akoğlu et al. (2018). In the first stage a simulated annealing nonlinear searching scheme followed by a derivative based method (Cervelli et al., 2001) is used to search for the fault geometry using a single fault with a uniform slip. In the second stage this fault is enlarged in both the strike and dip directions and then discretized into fault patches of 1 × 1 km. Through a linear inversion of the aforementioned subsampled set of InSAR measurements, a model with variable slip is then calculated. A nonnegativity constraint is applied for the linear inversion (Bro and Jong, 1997). Both datasets are given equal weights in the modeling and all parameters were set free except the width parameter that was given an upper bound of 5 km due to its trade-off with the dip-slip parameter. Even though the focal mechanism solutions from seismology indicate mostly a dominant normal mechanism for the earthquake, both dip and strike-slip components are solved for each fault patch. While it is generally a challenge to choose the right dip direction, especially for a Mw 5.2 earthquake, the distinct shape of the fringes that favor the mapped fault on the surface and the twofold increase in the overall root mean square values for a SW-dipping fault model aided in defining the dip direction of the fault.

The final model (Figure 5) suggests that a single 9 × 9 km fault can adequately explain the coseismic surface displacements (Figures 4a–4f). The rupture occurred along the northeast-dipping nodal plane and is confined only to the first 7 km. There are 2 main slip patches, each having a maximum slip of 30 cm with a slight right-lateral component. A dip of 52° provides the best fit to the ascending and descending InSAR data.

To estimate the uncertainties of the model parameters a Monte Carlo-based analysis is used in which the

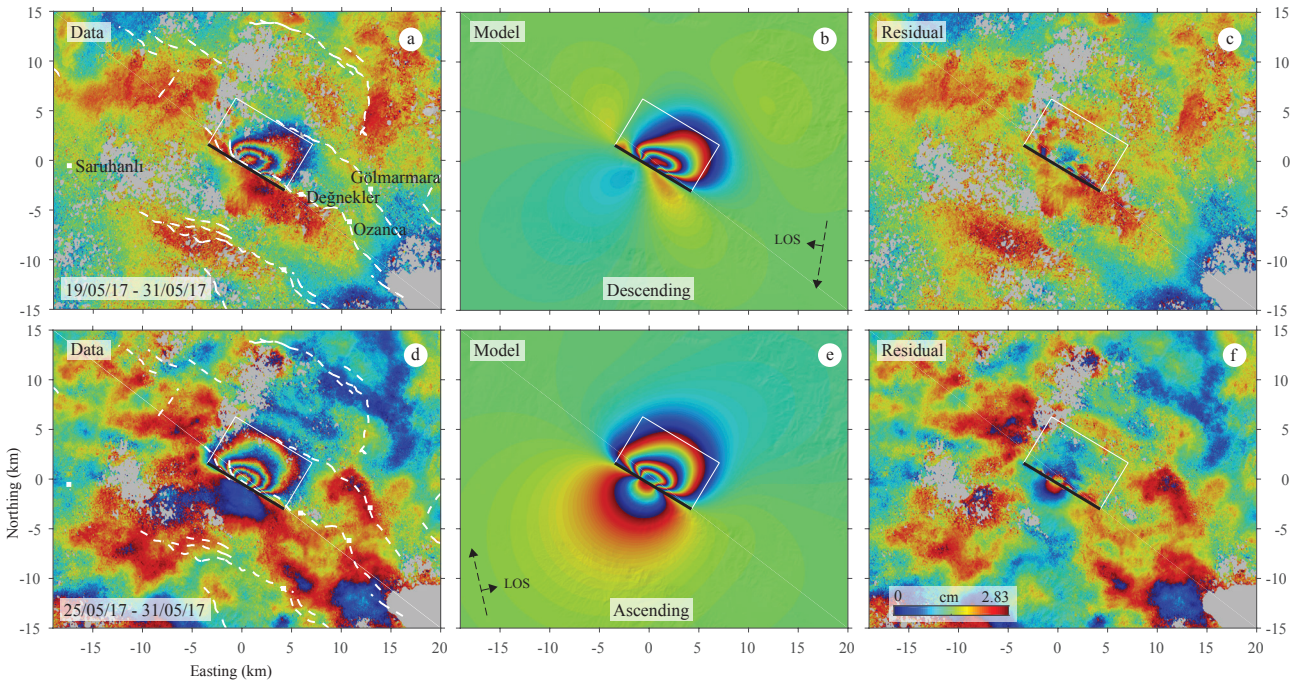

Figure 4. The comparison of the data, model, and residuals for the final model. Each fringe represents 2.83 cm of line-of-sight (LOS) deformation. The upper row (a–c) shows descending data, whereas the lower row (d–f) is for the Sentinel-1 data from the ascending orbit. The dashed white lines represent the active faults from Emre et al. (2018).The white rectangle represents the model fault plane with the thick black line depicting its up-dip edge. The black arrows indicate the flight direction of the radar satellite for each interferogram and the respective LOS direction for that orbit.

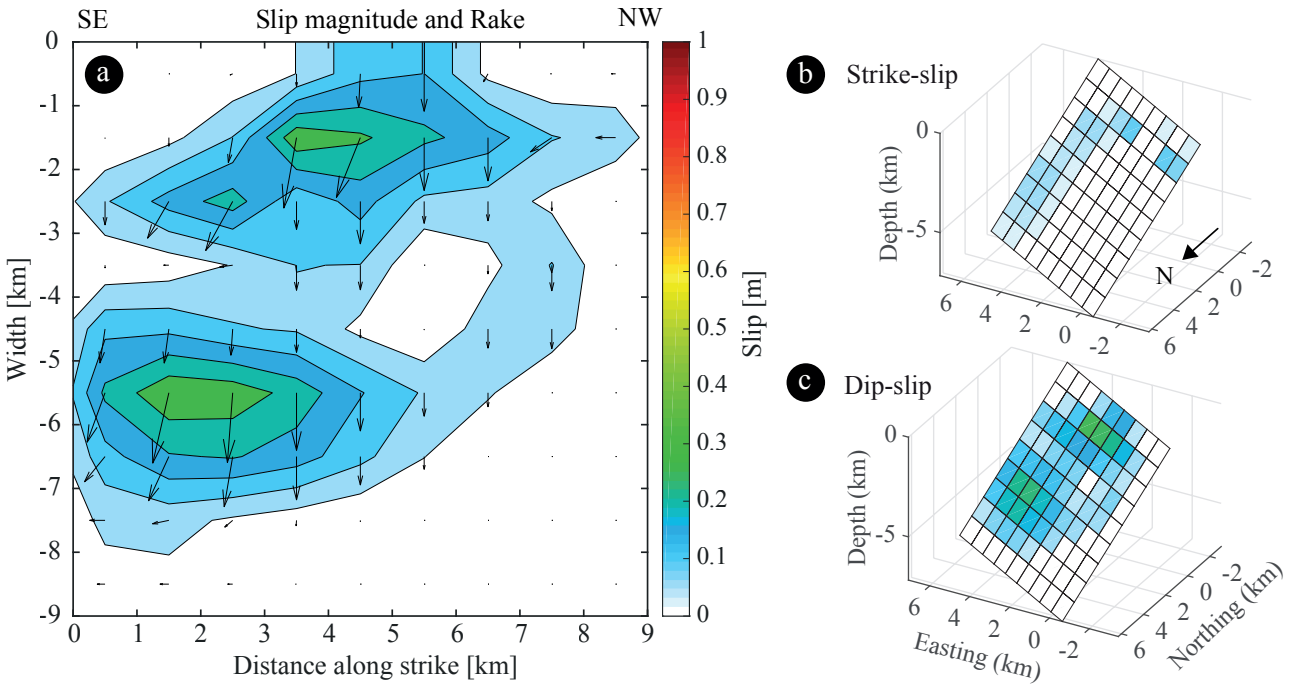

Figure 5. (a) The slip distribution for the best fitting fault model (Table 1). The black arrows show the rake directions for each fault patch. Existence of two slip patches hints that one of the two events on 28 May 2017 may have happened on the same fault plane as the mainshock. (b) The dip-slip component. (c) The strike-slip component of the final fault model. Easting and northing axes are local coordinates relative to 38.74°N, 27.77°E.

InSAR datasets are perturbed using random synthetic correlated noise. The noise characteristics are determined by calculating covariograms using data samples from the nondeforming regions of the interferograms. The 1D covariance models, which are fitted to the sample covariograms, are used to generate 100 perturbed datasets that are then inverted to assess the uncertainties of the model parameters (Figure 6). This also helps to identify the trade-offs between the parameters.

5. Coulomb stress changes

It is well known that static Coulomb failure stress (ΔCFF) increase caused by an earthquake may trigger subsequent earthquakes on neighboring faults (e.g., Stein et al. 1997; Toda et al., 1998). Even though the Coulomb stress changes caused by earthquakes are relatively smaller than the tectonic stresses required for an earthquake, Coulomb stress changes as low as 0.1 bar can be sufficient to trigger earthquakes (King et al., 1994). The Coulomb stress, ΔCFF, is defined as $\Delta CFF = \Delta\tau - \mu'\Delta\sigma$, where μ' is the apparent coefficient of friction and $\Delta\tau$ and $\Delta\sigma$ are the shear and normal stress changes, respectively (Stein et al., 1992). While an increase of Coulomb stress change will promote failures, a decrease will suppress it. In order to reveal the static stress transfer by the 27 May 2017 earthquake to the nearby faults, faults mapped by Emre et al. (2018) are digitized and then the Coulomb stresses resolved on them are calculated using the variable slip model (Figure 7). Coulomb 3.3 software (Toda et al., 2011) is used for the calculations assuming a fixed rake of –90 (i.e. pure normal faulting) and a coefficient of friction of 0.2 following Provost et al. (2003).

6. Discussion

As mentioned earlier, coseismic modeling shows that a single 9 × 9 km fault can adequately explain the geodetic data. The model fault's up-dip trace coincides with the northernmost half of the Ozanca Fault at the surface, whereas the rupture did not continue on to the southern half of the same fault. The slip on the model fault plane occurs in two main slip patches and diminishes below a depth of 7 km (Figure 5a), which is compatible with the reported values of the AFAD and USGS moment tensor solutions (Table 1). The Ozanca Fault is listed in the updated Active Tectonic Fault Map of Turkey (Emre et al., 2018) to have a dip of between 65° and 70°, slightly higher than the dip of the preferred model (52°). Since there were no field reports following the earthquake it is not possible to verify the ~10 cm of slip that the model resolves at the surface. There are no visible phase discontinuities in the interferograms indicating surface ruptures or triggered slip on nearby faults.

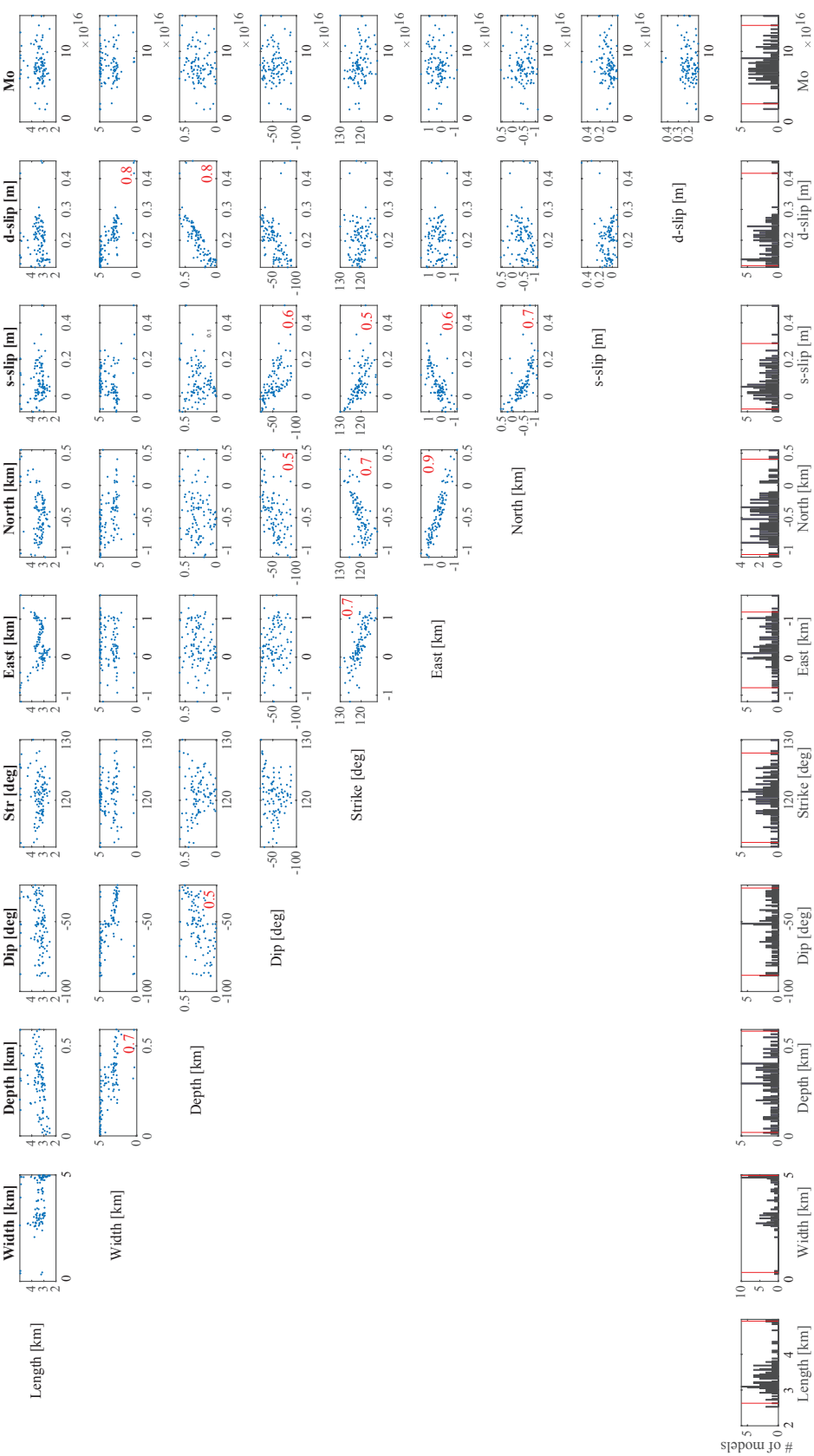

Figure 6. Model parameter distribution from 100 independent optimizations using uniform slip with added spatially correlated noise. The scatter plots of each pair of source parameters help to observe the trade-offs between the parameters while the numbers in red represent that the correlation coefficient between the parameters is over 0.5, emphasizing the presence of a trade-off (e.g., the trade-off between the depth and the dip-slip parameters). The bottom row shows the histograms for each parameter with the red vertical lines representing the 95% confidence interval bounds.

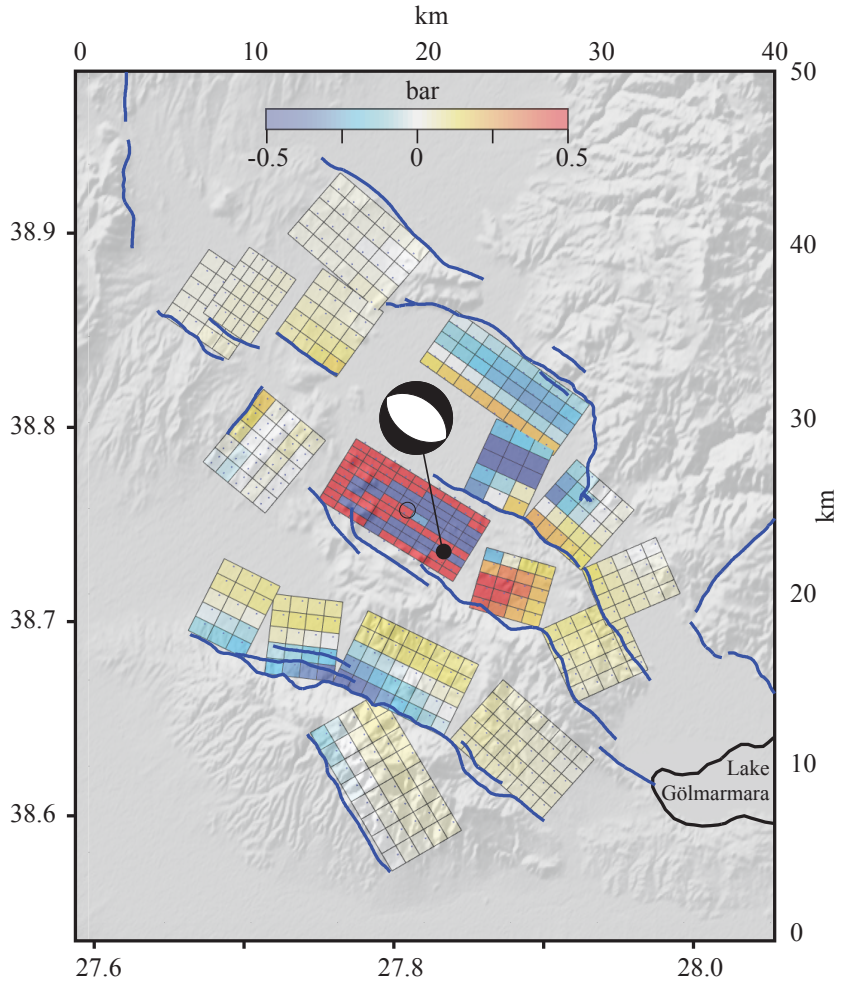

Figure 7. Coulomb stress changes resolved on nearby faults that are digitized from the updated active fault map of Turkey (Emre et al., 2018). The beachball represents the focal mechanism solution of the 27 May 2017 Mw 5.2 Saruhanlı earthquake from the Global CMT catalogue (Ekström et al., 2012).

The final model has a geodetic moment of 18.1×10^{16} Nm corresponding to a moment magnitude of 5.47, which is higher than the seismological estimates for the mainshock. This discrepancy should be due to the fact that both the ascending and descending interferograms used in the modeling captured not only the main Mw 5.2 event on May 27 but also the four subsequent events in the following day with magnitudes ranging from 4.5 to 5.0 (Figure 3; Table 1). The cumulated seismic moments of the mainshock and these four aftershocks are almost equal to the geodetic moment obtained from InSAR, implying that the recorded seismicity can adequately explain the geodetically observed deformation. There are two main slip patches in our final slip model (Figure 5a), and the slip on each patch has a moment equal to a Mw 5.2 earthquake. It can be proposed that one of these patches could be due to these events that have occurred along the Ozanca Fault following the mainshock on May 27.

As discussed earlier, the western (footwall block) side of the Ozanca Fault has a stronger atmospheric contribution than the eastern (hanging-wall block) side owing to the phase delays surrounding the Karadağ Hill. The descending model interferogram hints that part of this signal is due to the slip on the fault. This is the same for the ascending interferogram: the signal on the footwall block is overlapped with the phase delays due to the atmosphere.

Figure 6 shows the distribution of the model parameters and their uncertainties. There are apparent trade-offs between parameters like the depth and the dip-slip, width and the depth, and the strike and the location of the fault. The large width of the histogram for the dip parameter (Figure 6, bottom row) indicates that the parameter is poorly constrained with InSAR.

As seen in Figure 7, maximum Coulomb stress changes of over 1 bar occur on the unbroken sections of the Ozanca

Fault. Overall, the Coulomb stress change due to the earthquake increased the stress on all the neighboring faults, such as the Gölmarmara Fault to the east. However, note that on some of the faults the Coulomb stress change is both positive and negative, depending on the depth. While it is negative on shallow sections of some of the faults (e.g., those to the south), it becomes positive on the deeper parts.

With the introduction of the Sentinel-1 satellites, InSAR has become much more applicable for studying moderately sized events, especially the shallow earthquakes with a dip-slip mechanism such as the ones in western Turkey as emphasized in this study. InSAR-based studies focusing on the February 2017 earthquake sequence in the Biga Peninsula, Çanakkale (Ganas et al., 2018) and the April–November 2017 sequence in Ula, Muğla (Eskikoy et al., 2018) are other recent examples that took advantage of the improvement in the temporal coverage provided by the Sentinel-1 satellites to study the seismicity in western Turkey. Though deeper events like the 21 April 2017 Mw 5.1 Manisa-Şehzadeler earthquake (Figure 3) will still not be detected, it is apparent that future InSAR-based studies will improve our understanding of the secondary faulting in the region and the seismic hazard associated with them. In addition, the possibility of joint inversions of both seismological and geodetical datasets could help to improve fault parameter estimations. It is also worth mentioning that the atmospheric delays will continue to be the main drawback to hamper coseismic slip modeling. Taking advantage of the rich Sentinel-1 archive time series-based approaches could be useful to eliminate the noise due to atmospheric delays.

7. Conclusions

Our fault model based on InSAR data from both the ascending and descending orbits of the Sentinel-1 satellites shows that the 27 May 2017 earthquake occurred along the northeast dipping nodal plane. The NW-SE striking normal fault's up-dip trace coincides with the surface expression of the northernmost part of the Ozanca Fault; the rupture did not continue on to the southern segments. Modeling also shows that the coseismic slip during the May 2017 rupture on the Ozanca Fault is confined only to the first 7 km. Further detailed paleoseismological and geophysical studies are necessary to understand the Ozanca Fault's past earthquake activity, the down-dip extent of the fault plane, and its relation with the neighboring faults.

Acknowledgments

The interferograms presented in this study were calculated using Copernicus Sentinel-1 data [2017]. Most of the figures in this article were prepared using the Generic Mapping Tools (GMT) software package (Wessel et al., 2019). The TanDEM-X data are provided by the DRL under the scientific proposal IDEM_CALVAL0120.

References

AFAD DDA Catalog (2019). Ministry of the Interior, Disaster and Emergency Management Authority, Directorate of Earthquakes Catalog [online]. Website https://deprem.afad.gov.tr/ddakatalogu [accessed 01 December 2019].

Akoğlu AM, Jónsson S, Wang T, Çakır Z, Dogan U et al. (2018). Evidence for tear faulting from new constraints of the 23 October 2011 Mw 7.1 Van, Turkey, earthquake based on InSAR, GPS, coastal uplift, and field observations. Bulletin of the Seismological Society of America 108 (4): 1929-1946.

Aktug B, Nocquet JM, Cingöz A, Parsons B, Erkan Y et al. (2009). Deformation of western Turkey from a combination of permanent and campaign GPS data: limits to block-like behavior. Journal of Geophysical Research 114 (B10): B10404. doi: 10.1029/2008JB006000

Altikulac E (2015). Structure & tectonic evolution of the Caldag High and the Golmarmara Basin in the western Gediz Graben, western Anatolia. MSc, Miami University, Oxford, OH, USA.

Bro R, Jong SD (1997). A fast non-negativity-constrained least squares algorithm. Journal of Chemometrics 11: 9.

Cakir Z, Akoglu AM (2008). Synthetic aperture radar interferometry observations of the M 6.0 Orta earthquake of 6 June 2000 (NW Turkey): reactivation of a listric fault. Geochemistry, Geophysics, Geosystems 9 (8): Q08009. doi: 10.1029/2008GC002031

Cakir Z, Akoglu A, Belabbes S, Ergintav S, Meghraoui M (2005). Creeping along the Ismetpasa section of the North Anatolian fault (Western Turkey): rate and extent from InSAR. Earth and Planetary Science Letters 238 (1-2): 225-234. doi: 10.1016/j.epsl.2005.06.044

Çakir Z, de Chabalier JB, Armijo R, Meyer B, Barka A et al. (2003). Coseismic and early post-seismic slip associated with the 1999 Izmit earthquake (Turkey), from SAR interferometry and tectonic field observations. Geophysical Journal International 155 (1): 93-110. doi: 10.1046/j.1365-246X.2003.02001.x

Cavalié O, Jónsson S (2014). Block-like plate movements in eastern Anatolia observed by InSAR. Geophysical Research Letters 41 (1): 26-31. doi: 10.1002/2013GL058170

Cervelli P, Murray MH, Segall P, Aoki Y, Kato T (2001). Estimating source parameters from deformation data, with an application to the March 1997 earthquake swarm off the Izu Peninsula, Japan. Journal of Geophysical Research: Solid Earth 106 (B6): 11217-11237. doi: 10.1029/2000JB900399

Dewey JF, Şengör AMC (1979). Aegean and surrounding regions: Complex multiplate and continuum tectonics in a convergent zone. GSA Bulletin 90 (1): 84-92.

Dogan U, Demir DÖ, Çakir Z, Ergintav S, Ozener H et al. (2014). Postseismic deformation following the Mw 7.2, 23 October 2011 Van earthquake (Turkey): evidence for aseismic fault reactivation. Geophysical Research Letters 41 (7): 2334-2341. doi: 10.1002/2014GL059291

Ekström G, Nettles M, Dziewoński AM (2012). The global CMT project 2004–2010: Centroid-moment tensors for 13,017 earthquakes. Physics of the Earth and Planetary Interiors 200-201: 1-9. doi: 10.1016/j.pepi.2012.04.002

Emre Ö, Duman TY, Özalp S, Elmacı H, Olgun Ş et al. (2013). Açıklamalı Türkiye Diri Fay Haritası Ölçek: 1: 1.250.000. Ankara, Turkey: Maden Tetkik ve Arama Genel Müdürlüğü (in Turkish).

Emre Ö, Duman TY, Özalp S, Şaroğlu F, Olgun Ş et al. (2018). Active fault database of Turkey. Bulletin of Earthquake Engineering 16 (8): 3229-3275. doi: 10.1007/s10518-016-0041-2

Eski S (2014). Gölmarmara Havzasının (Gediz Grabeni Kuzey Kolu) Aktif Tektoniği, Manisa. MSc, Dokuz Eylül University, İzmir, Turkey (in Turkish).

Eskikoy F, Ergintav S, Özgün Konca A, Akoglu AM (2018). Source parameters of the 22-24 November 2017 Mugla earthquake sequence from seismology, GPS and InSAR. In: EGU General Assembly Conference Abstracts 20, 15099.

Funning GJ, Garcia A (2019). A systematic study of earthquake detectability using Sentinel-1 Interferometric Wide-Swath data. Geophysical Journal International 216: 332-349. doi: 10.1093/gji/ggy426

Ganas A, Kourkouli P, Briole P, Moshou A, Elias P et al. (2018). Coseismic displacements from moderate-size earthquakes mapped by Sentinel-1 differential interferometry: the case of February 2017 Gulpinar earthquake sequence (Biga Peninsula, Turkey). Remote Sensing 10 (7): 1089. doi: 10.3390/rs10071089

GEBCO Compilation Group (2019). GEBCO 2019 Grid. London, UK: GEBCO Compilation Group.

Jolivet L, Faccenna C, Huet B, Labrousse L, Le Pourhiet L et al. (2013). Aegean tectonics: Strain localisation, slab tearing and trench retreat. Tectonophysics 597-598: 1-33. doi: 10.1016/j.tecto.2012.06.011

Jónsson S, Zebker HA, Segall P, Amelung F (2002). Fault slip distribution of the 1999 Mw 7.1 Hector Mine, California, earthquake, estimated from satellite radar and GPS measurements. Bulletin of the Seismological Society of America 92 (4): 1377-1389. doi: 10.1785/0120000922

Kadirioğlu FT, Kartal RF, Kılıç R, Kalafat D, Duman TY et al. (2018). An improved earthquake catalogue (M ≥ 4.0) for Turkey and its near vicinity (1900-2012). Bulletin of Earthquake Engineering 16 (8): 3317-3338. doi: 10.1007/s10518-016-0064-8

Kavak KS (2005). Determination of palaeotectonic and neotectonic features around the Menderes Massif and the Gediz Graben (western Turkey) using Landsat TM image. International Journal of Remote Sensing 26 (1): 59-78. doi: 10.1080/01431160410001709994

Kavak KS, Cetin H (2007). A detailed geologic lineament analysis using Landsat TM data of Gölmarmara/Manisa Region, Turkey. Online Journal of Earth Sciences 1 (3): 145-153.

Koçyiğit A, Yusufoğlu H, Bozkurt E (1999). Evidence from the Gediz graben for episodic two-stage extension in western Turkey. Journal of the Geological Society 156 (3): 605-616. doi: 10.1144/gsjgs.156.3.0605

Konca AO, Leprince S, Avouac JP, Helmberger DV (2010). Rupture process of the 1999 Mw 7.1 Duzce earthquake from joint analysis of SPOT, GPS, InSAR, strong-motion, and teleseismic data: a supershear rupture with variable rupture velocity. Bulletin of the Seismological Society of America 100 (1): 267-288. doi: 10.1785/0120090072

Le Pichon X, Angelier J (1979). The Hellenic arc and trench system: a key to the neotectonic evolution of the eastern Mediterranean area. Tectonophysics 60 (1-2): 1-42. doi: 10.1016/0040-1951(79)90131-8

Le Pichon X, Angelier J (1981). The Aegean sea. Philosophical Transactions of the Royal Society of London. Series A, Mathematical and Physical Sciences 300 (1454): 357-372.

Le Pichon X, Kreemer C (2010). The Miocene-to-present kinematic evolution of the eastern Mediterranean and Middle East and its implications for dynamics. Annual Review of Earth and Planetary Sciences 38 (1): 323-351. doi: 10.1146/annurev-earth-040809-152419

McKenzie D (1972). Active tectonics of the Mediterranean Region. Geophysical Journal of the Royal Astronomical Society 30: 109-185.

McKenzie D (1978). Active tectonics of the Alpine-Himalayan belt: the Aegean Sea and surrounding regions. Geophysical Journal International 55 (1): 217-254. doi: 10.1111/j.1365-246X.1978.tb04759.x

Merryman Boncori JP (2019). Measuring coseismic deformation with spaceborne synthetic aperture radar: a review. Frontiers in Earth Science 7: 16. doi: 10.3389/feart.2019.00016

Murray KD, Bekaert DPS, Lohman RB (2019). Tropospheric corrections for InSAR: Statistical assessments and applications to the Central United States and Mexico. Remote Sensing of Environment 232: 111326. doi: 10.1016/j.rse.2019.111326

Özkaymak Ç, Sözbilir H, Uzel B (2013). Neogene–Quaternary evolution of the Manisa Basin: Evidence for variation in the stress pattern of the İzmir-Balıkesir Transfer Zone, western Anatolia. Journal of Geodynamics 65: 117-135. doi: 10.1016/j.jog.2012.06.004

Philippon M, Brun JP, Gueydan F, Sokoutis D (2014). The interaction between Aegean back-arc extension and Anatolia escape since middle Miocene. Tectonophysics 631: 176-188. doi: 10.1016/j.tecto.2014.04.039

Pondrelli S (2002). European-Mediterranean Regional Centroid-Moment Tensors Catalog (RCMT) [Data set]. Rome, Italy: Istituto Nazionale di Geofisica e Vulcanologia (INGV). doi: 10.13127/rcmt/euromed

Provost AS, Chéry J, Hassani R (2003). 3D mechanical modeling of the GPS velocity field along the North Anatolian fault. Earth and Planetary Science Letters 209 (3-4): 361-377. doi: 10.1016/S0012-821X(03)00099-2

Reilinger R, McClusky S, Paradissis D, Ergintav S, Vernant P (2010). Geodetic constraints on the tectonic evolution of the Aegean region and strain accumulation along the Hellenic subduction zone. Tectonophysics 488 (1-4): 22-30. doi: 10.1016/j.tecto.2009.05.027

Reilinger R, McClusky S, Vernant P, Lawrence S, Ergintav S et al. (2006). GPS constraints on continental deformation in the Africa-Arabia-Eurasia continental collision zone and implications for the dynamics of plate interactions. Journal of Geophysical Research: Solid Earth 111: B5. doi: 10.1029/2005JB004051.

Rosen PA, Gurrola EM, Agram PS, Sacco GF, Lavalle M (2015). The InSAR Scientific Computing Environment (ISCE): A Python Framework for Earth Science. In: AGU Fall Meeting Abstracts, San Francisco, CA, USA, Abstract IN11C-1789.

Royden LH (1993). The tectonic expression slab pull at continental convergent boundaries. Tectonics 12 (2): 303-325. doi: 10.1029/92TC02248

Şengör AMC (1987). Cross-faults and differential stretching of hanging walls in regions of low-angle normal faulting: examples from western Turkey. Geological Society of London Special Publications 28 (1): 575. doi: 10.1144/GSL.SP.1987.028.01.38

Şengör AMC (1978). Über die angebliche primäre Vertikaltektonik im Ägäisraum. Neues Jahrbuch für Geologie und Palaeontologie 11: 698-703 (in German).

Şengör AMC, Görür N, Şaroğlu F (1985). Strike-slip faulting and related basin formation in zones of tectonic escape: Turkey as a case study. In: Biddle KT, Christie-Blick N (editors). Strike-Slip Deformation, Basin Formation, and Sedimentation. Tulsa, OK, USA: Society of Economic Paleontologists and Mineralogists Special Publications, pp. 227-264.

Şengör AMC, Zabcı C (2019). The North Anatolian Fault and the North Anatolian Shear Zone. In: Kuzucuoğlu C, Çiner A, Kazancı N (editors). Landscapes and Landforms of Turkey. Berlin, Germany: Springer, pp. 481-494. doi: 10.1007/978-3-030-03515-0_27

Şentürk S, Çakır Z, Ergintav S, Karabulut H (2019). Reactivation of the Adıyaman Fault (Turkey) through the Mw 5.7 2007 Sivrice earthquake: an oblique listric normal faulting within the Arabian-Anatolian plate boundary observed by InSAR. Journal of Geodynamics 131: 101654. doi: 10.1016/j.jog.2019.101654

Seyitoğlu G, Scott B (1991). Late Cenozoic crustal extension and basin formation in west Turkey. Geological Magazine 128 (2): 155-166. doi: 10.1017/S0016756800018343

Seyitoğlu G, Scott BC, Rundle CC (1992). Timing of Cenozoic extensional tectonics in west Turkey. Journal of the Geological Society 149 (4): 533-538. doi: 10.1144/gsjgs.149.4.0533

Toda S, Stein RS, Sevilgen V, Lin J (2011). Coulomb 3.3 Graphic-Rich Deformation and Stress-Change Software for Earthquake, Tectonic, and Volcano Research and Teaching-User Guide: U.S. Geological Survey Open-File Report 2011-1060. Reston, VA, USA: USGS.

Wessel P, Luis JF, Uieda L, Scharroo R, Wobbe F et al. (2019). The Generic Mapping Tools Version 6. Geochemistry, Geophysics, Geosystems 20 (11): 5556-5564. doi: 10.1029/2019GC008515

Wright TJ, Parsons BE, Jackson JA, Haynes M, Fielding EJ et al. (1999). Source parameters of the 1 October 1995 Dinar (Turkey) earthquake from SAR interferometry and seismic bodywave modelling. Earth and Planetary Science Letters 172 (1-2): 23-37. doi: 10.1016/S0012-821X(99)00186-7